Proceedings of the Canadian Society for Mechanical Engineering International Congress
32nd Annual Conference of the Computational Fluid Dynamics Society of Canada
Canadian Society of Rheology Symposium
CSME/CFDSC/CSR 2025
May 25–28, 2025, Montréal, Québec, Canada

NUMBER

PHASE-FIELD CRACK SIMULATION FOR THERMOMECHANICALLY COUPLED PROBLEMS

Zhirou Hu[1], Kuiying Chen[2], Tao Jin[1*]

[1]Department of Mechanical Engineering, University of Ottawa, Ottawa, Canada
[2]Aerospace Research Centre, National Research Council Canada, Ottawa, Canada
[*]tao.jin@uottawa.ca

***Abstract*—**The phase-field approach is widely adopted for crack simulations due to its capability of naturally treating complex crack geometries such as merging and branching. Both the staggered approach based on the alternate minimization and the monolithic approach based on the limited-memory BFGS algorithm are developed for the phase-field crack simulations. Particularly, the limited-memory BFGS approach is introduced to overcome the convergence issues caused by the non-convex energy functional. This approach is further combined with a heat conduction problem to investigate the crack propagation under thermomechanically coupled conditions. Several numerical examples are provided to demonstrate the capabilities of the developed method, including crack simulations in the quenching problem and the thermal barrier coating problem. The performance of the developed method is also reported.

***Keywords-component*—phase-field method; crack propagation; thermomechanical coupling**

I. INTRODUCTION

Thermal induced fracture is a commonly encountered phenomenon in engineering problems. Typical examples include the quenching cracks [1] and crack propagation due to the mismatch of the coefficient of thermal expansion (CTE) between materials [2]. With the advancement of computational mechanics, many numerical methods for fracture simulation have been developed. For instance, based on classical finite element method, the virtual crack closure technique (VCCT) is relatively simple to implement [3]. However, the singularity of crack tips limits its utilization. The extended finite element method (XFEM) [4] uses extra shape functions within elements to describe the sharp discontinuity of cracks, and therefore, avoids remeshing of the computational domain. The challenge of the XFEM is that it needs to track the crack path, making it difficult to deal with complex cracks and their interaction.

In recent years, the phase-field method for crack simulation attracts more and more attention. The phase-field method is based on a variational approach proposed by Francfort and Marigo [5], and is further validated by Bourdin *et al.* [6]. Miehe *et al.* proposed a thermodynamically consistent model and a robust computational framework using the staggered algorithm [7, 8], which is also known as the alternate minimization (AM). Due to the non-convex nature of the underlying energy functional, the convergence issue is challenging for the phase-field method for crack simulation. Bourdin [6] mathematically proved that when either the phase-field or the displacement field is fixed, the total energy functional is convex. As a result, the AM method is a robust approach to overcome the convergence issues. On the other hand, the AM is extremely slow to converge. To overcome this issue, Wu *et al.* [9] advocated to use the monolithic approach based on the celebrated Broyden–Fletcher–Goldfarb–Shanno (BFGS) algorithm. Unlike the conventional Newton-based monolithic algorithm, the BFGS method can overcome the convergence issues caused by the non-convex energy functional while at the same time improve the efficiency of the nonlinear iterations compared with the AM method. The conventional BFGS scheme needs to store fully dense matrices, making it impractical for large-scale problems due to the memory requirement. To reduce the memory requirement, the limited-memory BFGS (L-BFGS) method is purposed by researchers [10, 11].

In this work, we first briefly overview the framework of the phase-field crack simulations. Then, we introduce the staggered approach based on the alternate minimization and the monolithic approach based on the L-BFGS scheme. We further

* corresponding author

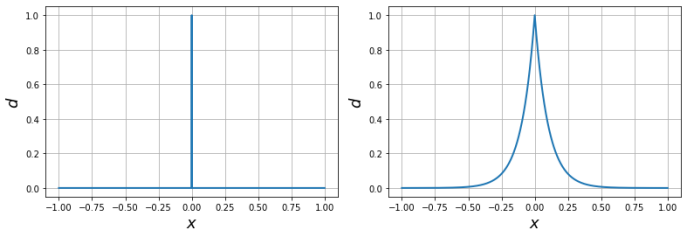

(a) Sharp crack topology (b) Diffusive crack representation

Figure. 1: 1D phase-field representation of the diffusive crack instead of the sharp crack.

incorporate the thermal effect into the modeling process. Crack simulations under both the mechanical and thermal loading are performed. We also apply the phase-field algorithm in a simple thermal barrier coating (TBC) system to demonstrate the potential for engineering applications.

II. Phase-field crack formulation

In this section, we first briefly overview the techniques for the diffusive representation of cracks. Then, we present the theoretical framework to model crack propagation using the phase-field approach. We further introduce the staggered approach and the monolithic approach as the solving technique for the phase-field crack problems.

A. Diffusive Crack

The basic idea of the phase-field method for crack modeling is to represent the sharp crack topology (discontinuity) in a diffusive manner [5]. Consider an one-dimension scenario shown in Fig. 1a, where a crack of the bar exists at the location of $x = 0$. This sharp crack can be represented by the phase-field $d(x) \in [0, 1]$, where $d = 0$ represents the intact (undamaged) state and $d = 1$ represents the crack (fully damaged) state. In order to avoid the numerical difficulties associated with the discontinuity of the phasefield, an alternative approach to represent the crack topology is to adopt the following exponential function as an approximation,

$$d = e^{-|x|/l} \tag{1}$$

where l is a length-scale parameter, as shown in Fig. 1b. As the length-scale parameter l goes to zero, the sharp crack topology can be recovered. This one-dimensional case can be generalized to 2D or 3D scenarios [7].

$$\begin{cases} d - l^2\nabla^2 d = 0 & \text{in } \Omega, \\ \nabla d \cdot \boldsymbol{n} = 0 & \text{on } \partial\Omega. \end{cases} \tag{2}$$

The corresponding weak form is obtained as

$$\int_\Omega \left[d\delta d + l^2(\nabla d) \cdot (\nabla \delta d)\right] \, \mathrm{d}V = 0.$$

The distribution of the phase-field $d(\boldsymbol{x})$ can be obtained by solving the linear system

$$\boldsymbol{K}\boldsymbol{d} = \boldsymbol{0},$$

$$K_{AB} = \int_\Omega \left[N_A N_B + l^2(\nabla N_A) \cdot (\nabla N_B)\right] \, \mathrm{d}V, \tag{3}$$

where N_A and N_A represent the finite element shape function.

Fig. 2 shows two cracks intersecting each other. The diffusive phase-field to represent the cracks is illustrated in Fig. 2a and 2b. In this case the adaptive mesh refinement(AMR) is applied such that fine meshes are only used around the crack region.

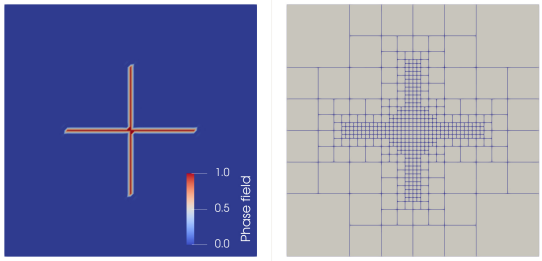

(a) Adaptively refined 4 times

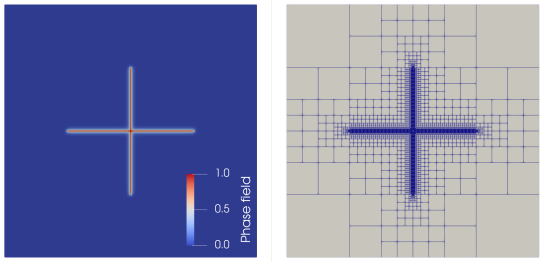

(b) Adaptively refined 9 times

Figure. 2: Phase-field representation of diffusive crack with adaptive mesh refinement technique.

B. Numerical Modeling of Crack Propagation

The energy functional of a cracked solid media can be written as

$$\begin{aligned} \Pi(\boldsymbol{u}, d) = &\int_\Omega \psi\left(\boldsymbol{\epsilon}(\boldsymbol{u}), d\right) \mathrm{d}\Omega + g_c \Gamma_l(d) \\ &- \int_\Omega \boldsymbol{b} \cdot \boldsymbol{u} \, \mathrm{d}\Omega - \int_{\partial\Omega} \boldsymbol{t} \cdot \boldsymbol{u} \, \mathrm{d}\Gamma, \end{aligned} \tag{4}$$

where $\boldsymbol{b}$ is the body force, $\boldsymbol{t}$ is the traction load, $\boldsymbol{\epsilon} = \nabla^{(s)}\boldsymbol{u}$ is the small deformation linear strain tensor, ψ represents the strain energy density function, g_c is the critical energy release rate, and Γ_l is an approximation of the crack surface area. Particularly, the approximated crack surface Γ_l is defined as

$$\Gamma_l(d) = \int_\Omega \gamma(d, \nabla d) \mathrm{d}\Omega = \int_\Omega \frac{1}{2l}\left(d^2 + l^2 \nabla d \cdot \nabla d\right) \mathrm{d}\Omega, \tag{5}$$

where $\gamma(d, \nabla d)$ is considered as the crack surface density function, and l is the phase-field length-scale parameter.

It is assumed that only the tensile stress contributes to the crack propagation, so it is necessary to separate the stress into tensile and compressive parts. One effective way is based on

the spectrum decomposition [12, 13]. Due to the existence of crack, a degradation function is introduced [8]:

$$g(d) = (1-d)^2. \tag{6}$$

The degradation function only impacts the tensile stress, so the corresponding elastic energy density becomes

$$\psi(\varepsilon, d) = g(d)\psi^+(\varepsilon) + \psi^-(\varepsilon), \tag{7}$$

where

$$\psi^{\pm}(\boldsymbol{\varepsilon}) = \lambda tr\langle[\boldsymbol{\varepsilon}]\rangle_{\pm}^2/2 + \mu tr[\boldsymbol{\varepsilon}_{\pm}^2].$$

The decomposition of the stress tensor is

$$\begin{aligned}\boldsymbol{\sigma} := \frac{\partial\psi(\boldsymbol{\varepsilon}, d)}{\partial\varepsilon} &= g(d)(\lambda tr\langle[\boldsymbol{\varepsilon}]\rangle_+\boldsymbol{I} + 2\mu\boldsymbol{\varepsilon}_+) \\ &\quad +(\lambda tr\langle[\boldsymbol{\varepsilon}]\rangle_-\boldsymbol{I} + 2\mu\boldsymbol{\varepsilon}_-).\end{aligned} \tag{8}$$

Based on the above energy functional, the weak form of the above phase-field approach is expressed as

$$\begin{cases} \displaystyle\int_\Omega \nabla^s\delta u\boldsymbol{\sigma}dV - \int_\Omega \delta u\boldsymbol{b}dV - \int_{\partial\Omega}\delta u\boldsymbol{t}dA = 0, \\ \displaystyle\int_\Omega \frac{g_c}{l}d\delta ddV + \int_\Omega g_c l\nabla\delta d\nabla\delta ddV + \int_\Omega \delta dg'(d)\mathcal{H}dV = 0, \end{cases}$$

where $\mathcal{H}$ represents the maximum magnitude of the positive strain energy history, which is adopted to enforce the phase-field irreversibility [7, 8].

C. Staggered Approach Based on the Alternate Minimization

At the k-th iteration, we fix the solution of the phase-field $\boldsymbol{d}^{(k)}$ and update the displacement field $\boldsymbol{u}^{(k)} \to \boldsymbol{u}^{(k+1)}$:

$$(\nabla^s\delta\boldsymbol{u},\, \boldsymbol{\sigma}(\boldsymbol{u}^{(k+1)}, \boldsymbol{d}^{(k)})) = (\delta\boldsymbol{u},\, \boldsymbol{b}) + (\delta\boldsymbol{u},\, \boldsymbol{t})_{\Gamma_t}. \tag{9}$$

Notice that the above equation itself is nonlinear and needs to be solved iteratively. After the updated displacement field $\boldsymbol{u}^{(k+1)}$ is obtained, we can then solve for the updated phase-field $\boldsymbol{d}^{(k+1)}$ according to

$$\begin{aligned}\frac{g_c}{l}(\boldsymbol{d}^{(k+1)},\, \delta\boldsymbol{d}) + g_c l(\nabla\boldsymbol{d}^{(k+1)},\, \nabla\delta\boldsymbol{d}) \\ = (-g'(d^{(k+1)})\mathcal{H}(\boldsymbol{u}^{(k+1)}),\, \delta\boldsymbol{d}).\end{aligned} \tag{10}$$

The above two equations are repeatedly solved until the convergence criteria are satisfied. For the detailed steps of the staggered approach, see [8].

D. Monolithic Approach Based on the L-BFGS Scheme

Instead of updating the phase-field and displacement field separately following the staggered approach, these two unknown fields can be solved simultaneously in a monolithic approach,

$$\begin{bmatrix}\boldsymbol{u}^{(k+1)} \\ \boldsymbol{d}^{(k+1)}\end{bmatrix} = \begin{bmatrix}\boldsymbol{u}^{(k)} \\ \boldsymbol{d}^{(k)}\end{bmatrix} + \alpha_k\boldsymbol{H}^{(k)}\begin{bmatrix}-\boldsymbol{R}_u^{(k)} \\ -\boldsymbol{R}_d^{(k)}\end{bmatrix} \tag{11}$$

where

$$\boldsymbol{R}_u = \left(\nabla^{(s)}\boldsymbol{N}_u,\, \boldsymbol{\sigma}\right) - (\boldsymbol{N}_u,\, \boldsymbol{b}) - (\boldsymbol{N}_u,\, \boldsymbol{t})_{\Gamma_t} \tag{12}$$

and

$$\boldsymbol{R}_d = \left(N_d,\, \frac{g_c}{l}d + g'(d)\mathcal{H}\right) + (\nabla N_d,\, g_c l\nabla d). \tag{13}$$

During the above L-BFGS monolithic scheme, the key step is to calculate the inverse of the BFGS matrix $\boldsymbol{H}^{(k)}$. The conventional BFGS update requires the storage of a fully dense matrix, which is impractical for large-scale finite element simulations due to the memory requirement. In order to overcome this issue, the limited-memory BFGS (L-BFGS) update only needs to store a list of vector-pairs from the most recent iterations. For the detailed process, see [14]. In order to ensure the positive-definiteness of the L-BFGS matrix, the line search parameter α_k in Eq. (11) is decided via the strong Wolfe conditions

$$f(\boldsymbol{x}_k + \alpha_k\boldsymbol{p}_k) \le f(\boldsymbol{x}_k) + c_1\alpha_k\boldsymbol{r}_k^{\mathrm{T}}\boldsymbol{p}_k, \tag{14}$$

$$\left|\boldsymbol{r}(\boldsymbol{x}_k + \alpha_k\boldsymbol{p}_k)^{\mathrm{T}}\boldsymbol{p}_k\right| \le c_2\left|\boldsymbol{r}_k^{\mathrm{T}}\boldsymbol{p}_k\right|, \tag{15}$$

with $0 < c_1 < c_2 < 1$.

E. Thermal Induced Fracture Problem

In many engineering applications, crack typically develops under a combination of external loads, such as mechanical load and thermal load. In order to perform the crack simulation for thermomechanically coupled problems, we first solve for the temperature field based on the Fourier's law from a heat conduction problem,

$$c\rho\frac{\partial T}{\partial t} = \kappa\nabla^2 T + q, \tag{16}$$

where T represents the unknown temperature field, c is the specific heat, ρ is the material density, κ is the thermal conductivity coefficient, and q is the heat source. The weak form of this equation is

$$\begin{aligned}\int_\Omega \delta Tc\rho\frac{\partial T}{\partial t}dV + \int_\Omega \delta\nabla T\kappa\nabla TdV \\ = \int_\Omega \delta Tqd V + \int_{\partial\Omega}\delta Thd A.\end{aligned} \tag{17}$$

After solving the above heat conduction problem, we can then either use the staggered approach or the monolithic approach to solve for the phase-field and the displacement field. Notice that in this scenario, the stress tensor not only depends on the displacement field and phase-field but also the temperature field, that is,

$$\boldsymbol{\sigma} = \boldsymbol{\sigma}(\boldsymbol{u},\, d,\, T) = \boldsymbol{\sigma}(\boldsymbol{\epsilon}(\boldsymbol{u}),\, d) - \mathbb{C} : \boldsymbol{I}\alpha_T(T - T_0), \tag{18}$$

where T_0 is the reference temperature and α_T is the coefficient of the thermal expansion. It is noticeable that the heat conduction problem is linear and the temperature distribution can be considered as an independent process from fracture. So, the strategy of solving the thermomechanically coupled problem is to decouple the temperature sub-problem in each time step, and solve for the temperature field. Once the temperature field is obtained, the thermal strain can be calculated, which is used to modify the equation for displacement and obtain the stress. The other two fields can then be calculated by either the staggered or monolithic approach described previously.

III. Numerical examples

Several numerical examples are provided to demonstrate the capability of the developed phase-field method to model crack propagation in this section. The first example shows the crack propagation under a purely mechanical loading condition. The second and the third examples demonstrate the crack propagation under thermal induced external loads. Lastly, the crack propagation inside a thermal barrier coating system is demonstrated. Material properties of the test cases 1∼3 are listed in Table I.

TABLE. I: Material properties for test cases 1∼3.

Test case	$\lambda\,(kN/mm^2)$	$\mu\,(kN/mm^2)$	$g_c\,(kN/mm)$
Plane with holes	1.94	2.45	2.28×10^{-3}
Cross shape	6.07×10^{-5}	9.1×10^{-5}	2.0×10^{-10}
Quenching	213.46	143.2	42.5×10^{-6}

A. Mechanical Fracture Problem

A classic fracture test shown in Fig. 3 is investigated to validate that the developed phase-field method is able to model crack propagation inside complex geometries. In this case, a rectangular specimen with three unsymmetric holes and a notch is under tension. A pulling load is applied uniformly on the top hole in vertical direction while the bottom hole is fixed. Fig. 3c reports the force-displacement curve obtained from the staggered approach and the monolithic approach, respectively. The load-displacement curve matches the results reported by Gerasimov *et al.* [16].

B. Thermal Induced Fracture Problem

1) Cross-shaped specimen: A quasi-static heat conduction problem studied in [17] is used here to verify the accuracy of the developed phase-field method. The top edge is heated from 0 °C to 10 °C and the bottom edge is cooled from 0 °C to -10 °C. Both the alternate minimization and the L-BFGS method show similar results as reported in [17]. It is noticeable that the results reported in the literature indicate that the staggered approach based on the alternate minimization (AM) displays a secondary crack at the left corner of the sample, which is also shown in our results, see Figs. 4. Moreover, we can see that both approaches have almost identical results regarding the crack path induced by the thermal load.

2) Quenching: A sudden cooling can induce a steep temperature gradient, which generates considerable large thermal stresses. As a result, quenching cracks might appear. In this case, a bar of brittle material is heated to 300 °C and then quenched in a 0 °C liquid. Based on the symmetry, only half of the rectangular bar is modeled, as shown in Fig. 5. We can see that multiple cracks appear due to the stresses generated by the steep temperature gradient after 75 ms.

3) Thermal barrier coating (TBC): A thermal barrier coating (TBC) specimen, as shown in Fig. 6, is uniformly cooled from 1200 °C to 0 °C. The material properties of different layers, including the top coat (TC), the thermally grown oxide (TGO), the bond coat (BC), as well as the interface layer between the TGO and BC, are reported in Table II [18]. Due to the periodic structure of the TBC system, the computational domain only contains one sinusoidal period with the periodic boundary conditions applied on the left and right edges. Fig. 7a shows that the initial crack appears at the interface between the TGO and BC layers during the cooling process. The crack further develops until it reaches to the left and right boundaries, as shown in Fig. 7b. We can see that the proposed phase-field approach can successfully model the crack propagation caused by the thermal induced stresses.

Figure 8 compares the number of nonlinear iterations required by the L-BFGS approach and the AM approach during each load step in a simple shear test [19]. The former, which is

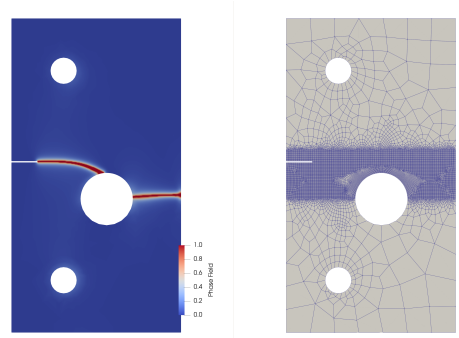

(a) Results based on the staggered approach (AM)

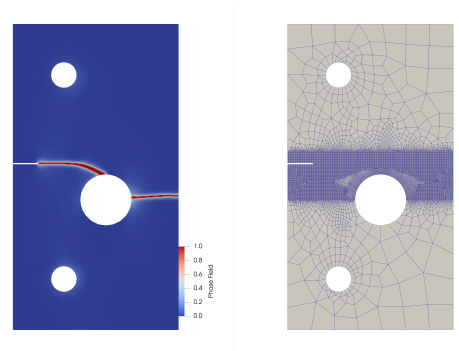

(b) Results based on the monolithic approach (L-BFGS)

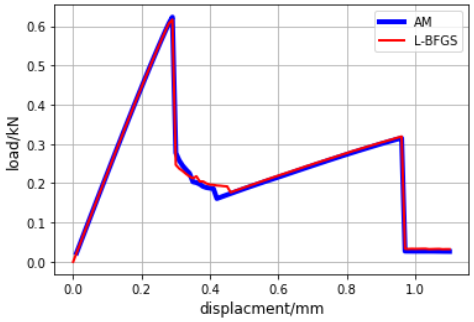

(c) Comparison of the load-displacement curves

Figure. 3: Plane with holes: comparing the load-displacement curves based on the staggered approach (AM) and the monolithic approach (L-BFGS).

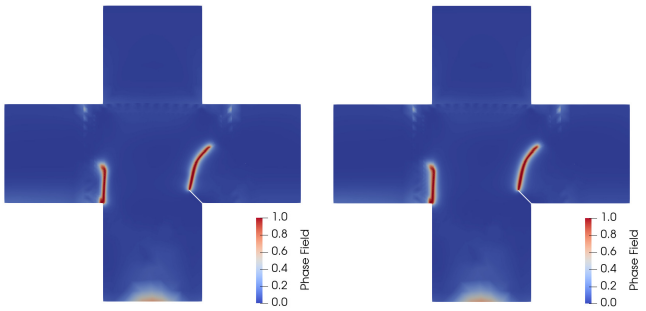

(a) Staggered approach (AM) (b) Monolithic approach (L-BFGS)

Figure. 4: Comparison of the thermal crack path obtained from the alternate minimization (AM) and the monolithic approach using the L-BFGS scheme.

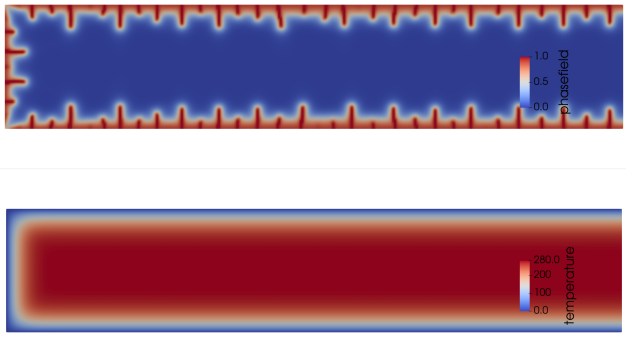

Figure. 5: Quenching cracks appear due to the large thermal stress caused by the steep temperature gradient.

TABLE. II: Material properties of TBC

Layer	$\lambda\,(kN/mm^2)$	$\mu\,(kN/mm^2)$	$g_c\,(kN/mm)$
TC	0.796	0.935	8×10^{-6}
TGO	96.6	122.95	50×10^{-6}
BC/TGO	126.92	84.62	10×10^{-6}
BC	126.92	84.62	300×10^{-6}

a type of monolithic solving strategy, requires fewer iterations for convergence than the staggered strategy using the alternate minimization (AM).

IV. Conclusions and Future Work

The phase-field approach is effective to model crack propagation in solid materials due to its capability of naturally handling complex crack geometries and the variational structure for the mathematical rigor. Conventional Newton-based methods encounter convergence issues due to the underlying non-convex energy functional. Two solving approaches are presented to overcome this issue, including the staggered approach based on the alternate minimization and the monolithic approach based on the limited-memory BFGS (L-BFGS)

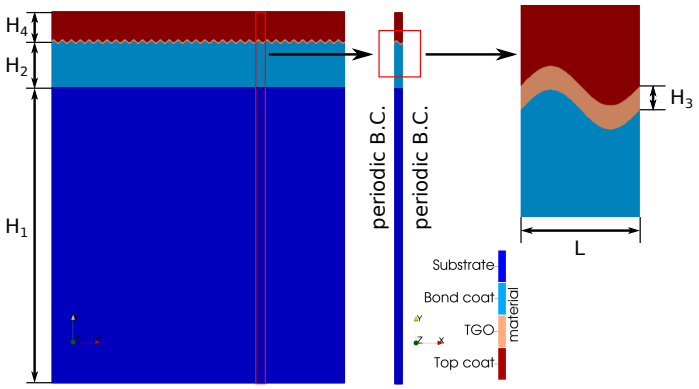

Figure. 6: Due to the periodic structure of the TBC system, the computational domain only contains one sinusoidal period with the periodic boundary conditions applied on the left and right edges.

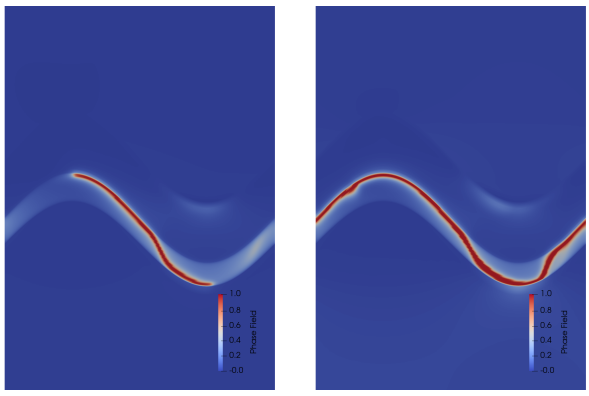

(a) Initial crack (b) Fully developed crack

Figure. 7: Crack at the interface between TGO and BC layers inside the thermal barrier coating caused by the cooling process.

scheme. The phase-field method is further expanded to consider the effect of thermal induced loading. Multiple numerical examples are provided to demonstrate its effectiveness for modeling crack propagation in thermomechanically coupled problems. There are several avenues to further improve the current method:

- Interface modeling: the multi-phase materials, i.e. TBC, typically involve both bulk and interfacial cracks. Our current example does not directly consider the interfacial effect, and instead, only uses a thin material region with a separate set of material properties. A common remedy is to use the cohesive zone model. For instance, Min et al. proposed a diffusive interface model [18], which is more compatible with the physical reality.
- Oxidation-diffusion modeling: one of the major causes of TBC failure is oxidation, which results in the TGO growth. The oxidation-diffusion equation can be used to describe the process of the TGO growth for long-term

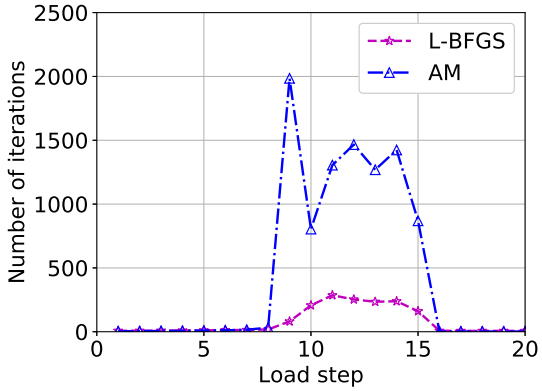

Figure. 8: Number of iterations required for convergence in each load step in a simple shear test problem. The L-BFGS approach, which is a type of monolithic solving strategy, requires fewer iterations than the staggered approach based on the alternate minimization (AM).

crack modeling.

- Parallel computing: in order to model 3D crack propagation in large-scale simulations, we plan to parallelize the presented numerical method via MPI to take advantage of modern computer architecture.

Acknowledgment

Tao Jin is supported by the Natural Sciences and Engineering Research Council of Canada (NSERC) under the Discovery Grants Program (funding reference number: RGPIN-2021-02561). Kuiying Chen is supported by the National Research Council Canada DTS-SCS program A1-018177 project. Their supports are greatly appreciated.

References

[1] Yingfeng Shao, et al. "Effect of crack pattern on the residual strength of ceramics after quenching." Journal of the American Ceramic Society 94.9 (2011): 2804-2807.

[2] Fu, Y. F., et al. "Thermal induced stress and associated cracking in cement-based composite at elevated temperatures—Part I: Thermal cracking around single inclusion." Cement and Concrete Composites 26.2 (2004): 99-111.

[3] Ronald Krueger. "Virtual crack closure technique: History, approach, and applications." Appl. Mech. Rev. 57.2 (2004): 109-143.

[4] Ted Belytschko and Tom Black. "Elastic crack growth in finite elements with minimal remeshing." International journal for numerical methods in engineering 45.5 (1999): 601-620.

[5] Gilles A. Francfort and J-J. Marigo. "Revisiting brittle fracture as an energy minimization problem." Journal of the Mechanics and Physics of Solids 46.8 (1998): 1319-1342.

[6] Blaise Bourdin, Gilles A. Francfort, and Jean-Jacques Marigo. "Numerical experiments in revisited brittle fracture." Journal of the Mechanics and Physics of Solids 48.4 (2000): 797-826.

[7] Christian Miehe, Fabian Welschinger, Martina Hofacker. "Thermodynamically consistent phase-field models of fracture: Variational principles and multi-field FE implementations." International journal for numerical methods in engineering 83.10 (2010): 1273-1311.

[8] Christian Miehe, Martina Hofacker, and Fabian Welschinger. "A phase field model for rate-independent crack propagation: Robust algorithmic implementation based on operator splits." Computer Methods in Applied Mechanics and Engineering 199.45-48 (2010): 2765-2778.

[9] Jian-Ying Wu, Yuli Huang, and Vinh Phu Nguyen. "On the BFGS monolithic algorithm for the unified phase field damage theory." Computer Methods in Applied Mechanics and Engineering 360 (2020): 112704.

[10] Jorge Nocedal. "Updating quasi-Newton matrices with limited storage." Mathematics of computation 35.151 (1980): 773-782.

[11] Dong C. Liu and Jorge Nocedal. "On the limited memory BFGS method for large scale optimization." Mathematical programming 45.1 (1989): 503-528.

[12] C. Miehe. "Comparison of two algorithms for the computation of fourth-order isotropic tensor functions." Computers & structures 66.1 (1998): 37-43.

[13] Christian Miehe and Matthias Lambrecht. "Algorithms for computation of stresses and elasticity moduli in terms of Seth–Hill's family of generalized strain tensors." Communications in numerical methods in engineering 17.5 (2001): 337-353.

[14] Tao Jin, Zhao Li, and Kuiying Chen. "A novel phase-field monolithic scheme for brittle crack propagation based on the limited-memory BFGS method with adaptive mesh refinement." International Journal for Numerical Methods in Engineering (2024): e7572.

[15] Tiancheng Zhang, et al. "Quasi-static thermoelastic fracture: Adaptive phase-field modeling with variable-node elements." Theoretical and Applied Fracture Mechanics 124 (2023): 103811.

[16] Tymofiy Gerasimov and Laura De Lorenzis. "A line search assisted monolithic approach for phase-field computing of brittle fracture." Computer Methods in Applied Mechanics and Engineering 312 (2016): 276-303.

[17] Tushar Kanti Mandal, et al. "Fracture of thermo-elastic solids: Phase-field modeling and new results with an efficient monolithic solver." Computer Methods in Applied Mechanics and Engineering 376 (2021): 113648.

[18] Lang Min, et al. "A chemo-thermo-mechanical coupled phase field framework for failure in thermal barrier coatings." Computer Methods in Applied Mechanics and Engineering 411 (2023): 116044.

[19] Tao Jin. "Gradient projection method for enforcing crack irreversibility as box constraints in a robust monolithic phase-field scheme." Computer Methods in Applied Mechanics and Engineering, 435:117622, 2025.